

# Topological equivalence of stripy states and skyrmion crystals

X. R. Wang,<sup>\*,†,‡</sup> Xu-Chong Hu,<sup>†,‡</sup> and Zhou-Zhou Sun<sup>¶,‡</sup>

<sup>†</sup>*Physics Department, The Hong Kong University of Science and Technology (HKUST), Clear Water Bay, Kowloon, Hong Kong*

<sup>‡</sup>*HKUST Shenzhen Research Institute, Shenzhen 518057, China*

<sup>¶</sup>*South China Business College, Guangdong University of Foreign Studies, Guangzhou 510545, China*

E-mail: phxwan@ust.hk

## Abstract

Stripy states, consisting of a collection of stripy spin textures, are the precursors of skyrmion crystals (SkXs). Common belief is that stripy states and SkXs are topologically unconnected, and transitions between SkXs and stripy states are phase transitions. Here, we show that both stripy states and SkXs are skyrmion condensates and they are topologically equivalent. By gradually tuning the stripe whose width goes from smaller than to larger than skyrmion-skyrmion separation, the structure of a skyrmion condensate transforms smoothly and continuously from various stripy phases, including helical states and mazes, to crystals, showing that stripy states are topologically connected to SkXs.

## Keywords

Nano-magnetism, chiral magnets, topological physics, skyrmion crystals, helical states

Magnetic skyrmions have attracted much attention in recent years for their academic interest and potential applications.<sup>1-8</sup> Various aspects of magnetic skyrmions have been extensively and intensively studied.<sup>9-46</sup> Vast experiments<sup>47</sup> showed that various stripy phases, including the helical states and mazes, accompany skyrmion crystals (SkXs). General belief is that stripy states and SkXs are topologically unconnected,<sup>47,48</sup> and transformations between them are phase transitions. Testing this belief motivates current study.

For a perpendicularly magnetized chiral film described by magnetization  $\mathbf{M}$ , the Heisenberg exchange stiffness constant  $A$ , anisotropic coefficient  $K$ , and the Dzyaloshinskii-Moriya interaction (DMI) coefficient  $D$ ,  $\kappa \equiv (\pi^2 D^2)/(16AK) = 1$ , an important quantity, separates isolated skyrmions ( $\kappa < 1$ ) from condensed stripe skyrmions ( $\kappa > 1$ ) in the absence of a magnetic field.<sup>49-52</sup> In this paper, we study how the morphology of a collection of stripe skyrmions changes as the stripe widths gradually increase. Our results show the topological equivalence of stripy states and SkXs and raise the question about the notion of the first-order phase transition in SkX formations.

We first investigate how morphology of 50 skyrmions, in films of  $400 \text{ nm} \times 400 \text{ nm} \times 0.5 \text{ nm}$ , changes with stripe width. Previous study<sup>49</sup> showed that one nucleation domain in a chiral magnetic film of  $\kappa = (\pi D)^2/(16AK) > 1$  develops into a stripe skyrmion. Thus, 50 nucleation domains of  $m_z = 1$  embedded in the  $m_z = -1$  background of chiral magnetic films can be used to generate 50 skyrmions. The 50 domains of 6 nm in diameter each are initially distributed in films randomly as shown in Fig. 1(a1). Figure 1(a2) shows a stable structure of 50 skyrmions for Film 1 with  $A/D = 1 \text{ nm}$  (a2). All stripes have the same width satisfying  $L = a(\kappa)A/D$  with  $a(\kappa = 2) = 6.5$ .<sup>49</sup>  $2L = 13 \text{ nm}$  for Film 1 is much smaller than average skyrmion-skyrmion separation  $d_{ss} = \sqrt{400 \times 400/50} \simeq 57 \text{ nm}$ . Since each nucleation domain has a large enough space to grow independently, the final stable structure is a dense maze formed by 50 ramified/non-ramified stripe skyrmions. Figures 1(a3) is a stable structure for Film 3 of  $A/D = 2 \text{ nm}$  and the dense maze becomes an irregularly arranged 42 stripe skyrmions and 8 circular-like skyrmions. Figures 1(a4)-(a6) are stable structures for Film 5 with  $A/D = 3 \text{ nm}$  (a4); Film 7 with  $A/D = 4 \text{ nm}$  (a5);

and Film 9 with  $A/D = 5$  nm (a6). Figures 1(a4)-(a5) are the mixtures of 20 circular skyrmions and 30 stripe skyrmions when  $L = 13.02$  nm (a4), 40 circular skyrmions and 10 stripe skyrmions when  $L = 26.04$  nm (a5), respectively. SkXs of 50 circular skyrmions form when  $2L$  is larger than 57 nm as shown in Fig. 1(a6). These results demonstrate the importance of  $L/d_{ss}$ .  $L/d_{ss} = 0.5$  roughly separates SkXs from mixture of stripe skyrmions and circular skyrmions, as shown in the  $L/d_{ss}$  phase diagram.

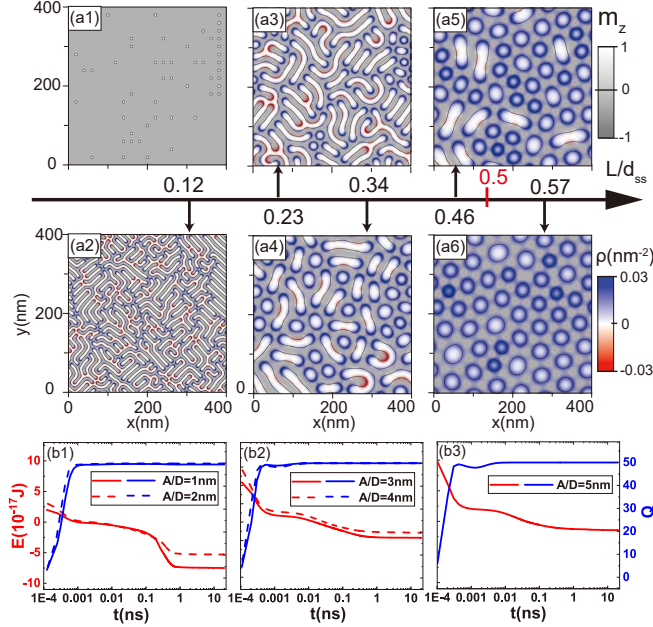


Figure 1: (a1) Initial configuration of randomly distributed 50 circular nucleation domains of  $m_z = 1$ . The diameter of each domain is 6 nm. (a2)-(a6) The stable spin structures with different  $A/D$ , starting from initial configuration (a1).  $A/D = 1$  nm (a2), 2 nm (a3), 3 nm (a4), 4 nm (a5), 5 nm (a6), corresponding to Films 1, 3, 5, 7, and 9 in Tab. 1.  $\kappa = 2$  for all films.  $L/d_{ss}$  shows the phase-diagram. (b1)-(b3) The time dependences of skyrmion number  $Q$  (the right y-axis and the blue curves) and total magnetic energy  $E$  (the left y-axis and the red curves).  $A/D = 1$  nm, 2 nm (b1); 3 nm, 4 nm (b2); 5 nm (b3). The time is in the logarithmic scale. All  $Q$  reaches the expected 50 within 1 ps, and  $E$  approaches its minimum in nanoseconds.

Interestingly, both positive and negative skyrmion charges, whose density is defined as  $\rho = \frac{1}{4\pi} \mathbf{m} \cdot (\partial_x \mathbf{m} \times \partial_y \mathbf{m})$ , appear in a stripe skyrmion while circular skyrmions carry only positive charges. The colours in Figs. 1(a2)-(a6) encode skyrmion charge (positive in blue and negative in red) distribution. Indeed, each small domain of initial zero skyrmion number becomes a skyrmion of  $Q = \int \rho dx dy = 1$  within 1 picoseconds. Each pattern in Figs. 1(a2)-(a6) consists of 50

skyrmions, evident from the time-dependence of  $Q(t)$  in Figs. 1(b1)-(b3).  $Q(t)$  reaches 50 within picoseconds. The total energy  $E$  monotonically decreases with time and approaches its minimal values in nanoseconds for all films as shown in Figs. 1(b1)-(b3) (the left y-axis and the red curves).

In the second set of simulations, starting from the stable maze structure of Fig. 1(a2) with 50 ramified stripe skyrmions for Film 1 of  $A/D = 1$  nm as the initial configuration, we consecutively increase  $A$  by 0.5 pJ/m and decrease  $K_u$  by proper values to keep  $\kappa = 2$  every 20 ns to simulate Film 2 to Film 10 listed in Tab. 1. Figures 2(a1)-(a6) are the stable structures for Film 2, 3, 4, 5, 7, and 9, respectively. Each of them comes from the stable structure of its predecessor. The time-dependences of  $E$  and  $Q$  are plotted in Fig. 2(b), showing that systems reach their equilibrium states (constant  $E$  and  $Q$ ) within a few nanoseconds with new set of parameters.  $Q = 50$  holds all the time due to the topological nature of the quantity.

For a given spin structure, the total magnetic energy is, according to Eq. (4) (see Methods),

$$\begin{aligned}
E &= d \int \int \{A|\nabla\mathbf{m}|^2 + D[m_z\nabla\cdot\mathbf{m} \\
&\quad - (\mathbf{m}\cdot\nabla)m_z] + K(1 - m_z^2)\}dxdy \\
&= \frac{\pi^2 D^2 d}{16A} \int \int \left\{ \frac{4A}{\pi D} |\nabla\mathbf{m}|^2 + \frac{4}{\pi} [m_z \frac{4A}{\pi D} \nabla\cdot\mathbf{m} \right. \\
&\quad \left. - (\mathbf{m}\cdot\frac{4A}{\pi D}\nabla)m_z] + \frac{1}{\kappa}(1 - m_z^2) \right\}dxdy \\
&= \kappa K d L^2 \int \int \left\{ |\nabla\mathbf{m}|^2 + \frac{4}{\pi} [m_z \nabla\cdot\mathbf{m} \right. \\
&\quad \left. - (\mathbf{m}\cdot\nabla)m_z] + \frac{1}{\kappa}(1 - m_z^2) \right\}dxdy.
\end{aligned} \tag{1}$$

Metastable spin structures depend only explicitly on  $\kappa = (\pi D)^2/(16AK)$ , and inexplicitly on the length scale of  $L_1 = 4A/(\pi D)$ . Since the integral area is shrunk by  $L_1^2$ , the total magnetic energy is proportional to  $\kappa K \propto D^2/A$  in the case of constant  $\kappa$ . Symbols in the inset of Fig. 2(b) are the total magnetic energies of metastable states for  $A/D = 1$  nm up to 5 nm. The solid curve is the fit to  $E(A/D) = cD^2/A$ , showing excellent agreement with simulations. The energy deviates slightly from  $cD^2/A$  for larger  $A/D$  such that  $L$  ( $L_1$ ) is comparable to skyrmion-skyrmion separation and skyrmion interactions becomes important.

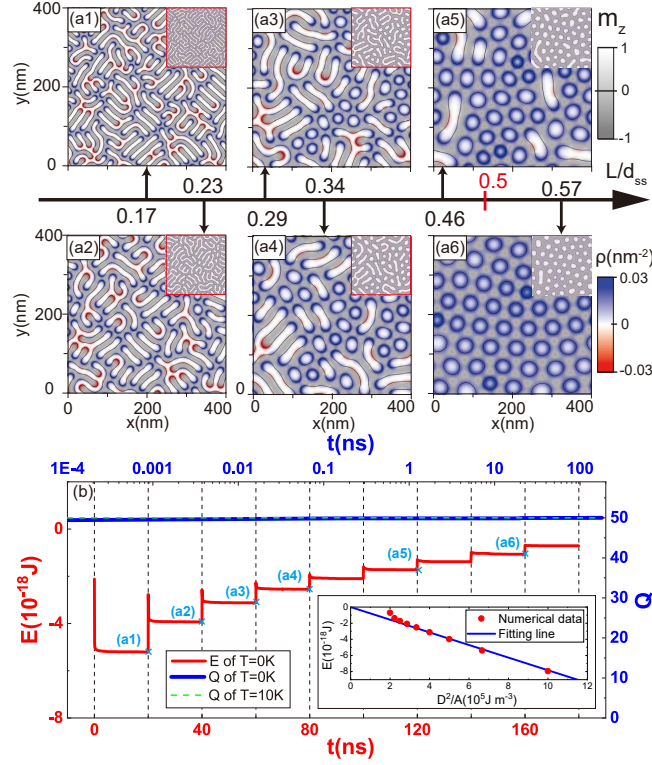


Figure 2: (a1) Stable structure of Film 2 developed from the stable structure of Film 1 of Fig. 1(a2). (a2) Stable structure of Film 3 of  $A/D = 2$  nm developed from (a1). (a3) Stable structure of Film 4 of  $A/D = 2.5$  nm from (a2). (a4) Stable structure of Film 5 of  $A/D = 3$  nm from (a3). (a5) Stable structure of Film 7 of  $A/D = 4$  nm. (a6) Stable structure of Film 9 of  $A/D = 5$  nm.  $\kappa = 2$  is for all films. Insets: Stable structures at temperature of 10 K for Film 3 (a2); Film 4 (a3); Film 5 (a4); Film 7 (a5); Film 9 (a6).  $L/d_{ss}$  shows the phase-diagram. (b) The blue line (0 K) and the green dash line (10 K) are the time evolution of skyrmion number  $Q$  (the right y-axis). The time is in the logarithmic scale (up x-axis). The red curve is the total energy  $E$  (the left y-axis) as a function of time in the normal scale (down x-axis).  $E$  for structures in (a1)-(a6) are marked by cross.  $Q$  maintains at 50 for both zero temperature and 10 K.  $E$  approaches a constant in nanoseconds after tuning the parameters. The inset is total magnetic energy of the stable structure as a function of  $D^2/A$ . The symbols are the simulation results and the blue curve is the fit to  $E = c(D^2/A)$  with  $c = (-7.8 \times 10^3 \text{ nm}^3)$ .

The spikes in  $E$ -curve come from sudden energy increase when parameters are modified. The energy of the new stable structure is higher (less negative) as  $A$  increases. Compare Fig. 2(a2) with Fig. 1(a3) for Film 3, Fig. 2(a4) with Fig. 1(a4) for Film 5, and Fig. 2(a5) with Fig. 1(a5) for Film 7, each pair has similar, but not identical, stable structures, revealing the fact of a large number of metastable structures for a collection of stripe skyrmions. Which metastable structure that a mixture of circular and stripe skyrmions ends up depends on the history of the system, see more discussions on this issue in Supporting Information.

Mumax3 simulations<sup>53</sup> at  $T = 10$  K, much lower than the Curie temperatures  $T_c$  (84 K~ 290 K for Film 2 to Film 9), are used to demonstrate the thermal stability, see Supporting Information for the detail of determining  $T_c$ . The insets of Fig. 2(a1)-(a6) are the metastable structures of Film 2 at 20ns (a1), Film 3 at 40ns (a2), Film 4 at 60ns (a3), Film 5 at 80 ns (a4), Film 7 at 120 ns (a4), and Film 9 at 160 ns (a6).  $Q = 50$  hold throughout 180 ns and morphology of the final states are similar as those at zero temperature for all films as shown in Fig. 2(b). However, one distinct difference is that skyrmion surfaces are more irregular and rough at finite temperatures, agreeing with experiments,<sup>54</sup> which may be understood from the negative skyrmion formation energy. Negative formation energy means negative surface tension such that such a surface can hardly resist external perturbations and deformations.

In contrast to a large number of metastable structures in stripe skyrmion condensate, variations of structures in SkXs are limited to a global translational transformation of all skyrmions. This explains why SkXs in Figs. 2(a6) and 1(a6) are almost the same although their kinetic and dynamical process are not the same. To further verify the independence of SkXs on their initial configurations, we repeat the simulations for Film 1, starting with the same 50 nucleation domains as those in Fig. 1 but arranged in two well-ordered columns as shown in Fig. 3(a1). Figure 3(a2) is the stable helical state after 20 ns evolution with 50 stripe skyrmions ( $Q(t) = 50$ ) as shown in Fig. 3(b)). Stripes tilt about  $56^\circ$  from the  $y$ -direction. The stripe tilt comes from film tiling by 25 stripes of width  $L \simeq 6.5$  nm. The tilted angle  $\theta$  satisfies  $2L/(\sin \theta) = 400/25$ . For  $L = 6.5$  nm,  $\theta = \cos^{-1}(13/16) \simeq 54^\circ$ , very close to the observed value of  $56^\circ$ .

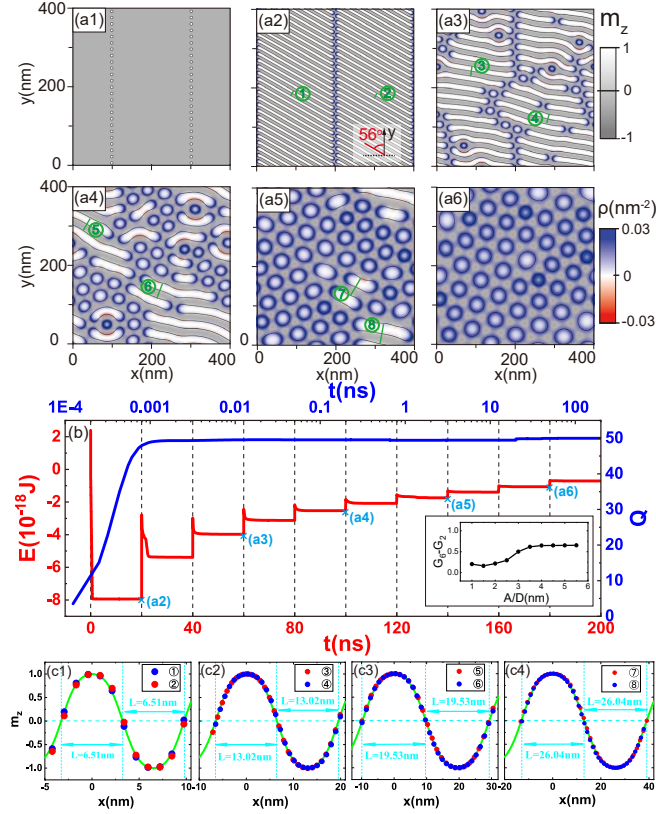


Figure 3: (a1) Initial configuration of 50 circular nucleation domains of  $m_z = 1$  arranged orderly in two columns. The diameter of each domain is 6 nm. (a2)-(a6) Stable structures for  $A/D = 1$  nm (a2); 2 nm (a3); 3 nm (a4); 4 nm (a5); and 5 nm (a6). All films have  $\kappa = 2$ . (b) The time evolution of skyrmion number  $Q$  (the right y-axis and the blue curve). Time is in the logarithmic scale (the top x-axis). The red curve is the total energy  $E$  (the left y-axis) as a function of time in the linear scale (the bottom x-axis).  $Q$  reaches 50 within 1 ps and keeps this value afterward even when the parameters are tuned to different values.  $E$  for structures in (a2)-(a6) are marked by cross. The inset is the  $A/D$  dependence of  $G_6 - G_2$ . (c1)-(c4) The red and the blue points are the z-component of magnetization along the green lines labeled by circled  $n$  in (a2)-(a5). The green lines are the fit to our approximate profile. The cyan arrows indicate the stripe widths of  $m_z < 0$  or  $m_z > 0$ .

After consecutively changing model parameters listed in Tab. 1 for Film 3 to 10 every 20 ns, Figs. 3(a3)-(a6) show stable structures for Film 3 with  $A/D = 2$  nm at 60 ns (a3), Film 5 with  $A/D = 3$  nm at 100 ns (a4), Film 7 with  $A/D = 4$  nm at 140 ns (a5), and Film 9 with  $A/D = 5$  nm at 180 ns (a6). Figure 3(b) shows time-dependences of  $E$  and  $Q$ . The spikes in  $E$ -curve are from the sudden change of model parameters.  $Q$  maintains the value of 50 after the first a few picoseconds while  $E$  reaches its minimal value in nanoseconds every time after parameter changes. The number of stripe (circular) skyrmions decreases (increases) as  $L$  increases. All skyrmions in Fig. 3(a6) are circular when  $L$  is larger than the average skyrmion-skyrmion separation.

To demonstrate that structure transformation from stripy states to SkXs is smooth, we introduce a local orientation order parameter, widely used in studying triangular lattices,<sup>55-57</sup> for  $i$ 'th skyrmion

$$\Psi_n(i) = \sum_{NN} e^{in\theta_{ij}}. \quad (2)$$

$\theta_{ij}$  is the angle of the direction from the center of skyrmion  $i$  to the center of skyrmion  $j$  with respect to the x-axis, and sum is over all nearest neighbouring skyrmions  $j$ . For a lattice with orientation order of a triangular lattice,  $\Psi_6(i)$  is close to 1 while it is a small complex number for a lattice without orientation order. For an imperfect lattice structure, averaged  $\Psi_n$  (over all skyrmions), called  $G_n$ ,

$$G_n = \frac{1}{N} \sum_i \Psi_n(r_i) \Psi_n^*(r_i), \quad (3)$$

can distinguish one skyrmion structure from another.<sup>55-57</sup>  $G_6$  for a SkX in a perfect triangular lattice is 1. Since  $G_6$  is also close to 1 for ordered stripe states such as those in Figs. 3(a2)-(a3), we use  $G_6 - G_2$ , which is close to 0 for a helical state and 1 for a SkX, as an order parameter to distinguish the two structures.  $G_6 - G_2$  undergoes a sudden transition for a first-order phase transition and a smooth variation for a non-phase transition. The inset of Fig. 3(b) shows how  $G_6 - G_2$  varies with  $A/D$  from 0 for an ordered stripe skyrmion state, via maze and mixture of stripes and circular skyrmions, to 1 for SkXs. The smooth variation of  $G_6 - G_2$  further supports the assertion of no first-order phase transition from helical states to SkXs. It should be pointed out



that our SkXs, similar to those in the literature, are not in perfect triangular lattice and  $G_6 - G_2$  is smaller than 1.

Previous studies<sup>49-52</sup> showed that stripe skyrmion structure follows  $m_z(x) = \frac{\sinh^2(L/2w) - \sinh^2(x/w)}{\sinh^2(L/2w) + \sinh^2(x/w)}$  for  $-L/2 < x < L/2$  and  $m_z(x) = -\frac{\sinh^2(L/2w) - \sinh^2(x/w - L/w)}{\sinh^2(L/2w) + \sinh^2(x/w - L/w)}$  for  $L/2 < x < 3L/2$ , where  $L$  and  $w$  are the stripe width and wall thickness.  $x = 0$  refers to stripe center where  $m_z = 1$ . Figures 3(c1)-(c4) are the distributions of  $m_z$  along lines labelled by the green @ in Figs. 3(a2)-(a5). The solid curves are the fits to the theoretical spin profile with  $L = 6.51$  nm and  $w = 1.73$  nm for (c1);  $L = 13.02$  nm and  $w = 3.46$  nm for (c2);  $L = 19.53$  nm and  $w = 5.19$  nm for (c3);  $L = 26.04$  nm and  $w = 6.92$  nm for (c4).  $L$  agrees perfectly with  $L = 6.51A/D$  for  $\kappa = 2$ . Data from different stripes falling onto the same curve demonstrates that stripes, building blocks of stripy pattern, are identical. Although the initial configurations in Figs. 1, 2, and 3 are different, and the morphologies of the mixtures of stripe and circular skyrmions are sensitive to the initial configurations and their dynamical paths, the structures of SkXs do not depend on the dynamical paths and depend only on the ratio of the stripe width and skyrmion-skyrmion separation.

To further substantiate the assertion above, we carry out similar simulations as those for Fig. 2, but with 100 randomly distributed nucleation domains as the initial configuration. The average skyrmion-skyrmion separation is reduced to  $d_{ss} = \sqrt{400 \times 400 / 100} = 40$  nm. Thus, we should expect the transformation from maze to the mixture of stripe and circular skyrmions, and to a SkX at smaller  $A/D$  than those in Fig. 2. As shown in Fig. 4, this is indeed the cases. (a1) is the initial configuration of randomly distributed 100 circular nucleation domains. (a2) is the stable structure of Film 1 of  $A/D = 1$  nm and  $\kappa = 2$  after 20 ns evolution. Clearly, it is a maze of 100 skyrmions, evident from  $Q = 100$  within a few picoseconds of evolution, and individual skyrmion is an irregular ramified stripe, or a curved or short stripe. After consecutive changes of  $A$  and  $K$  to simulate Films 3 to 10 given in Tab. 1 every 20 ns, Figs. 4(a3)-(a9) are their stable structures at  $t = 40$  ns; 60 ns; 80 ns; 100 ns; 120 ns; 140 ns; and 160 ns respectively for  $A/D = 1.5$  nm (a3);  $A/D = 2$  nm (a4); 2.5 nm (a5); 3 nm (a6), 3.5 nm (a7), 4 nm (a8), and 4.5 nm (a9) with stripe width  $L = 9.76$  nm, 13.02 nm, 16.27 nm, 19.53 nm, 22.78 nm, 26.04 nm, 29.29 nm, 32.55 nm. Indeed,

100 skyrmions form SkXs when  $A/D > 3$  nm as shown in Figs. 4(a7)-(a9), smaller than 4 nm in Fig. 2. For  $A/D = 3$  nm, almost all skyrmions are circular except 9 very short stripe skyrmions (a6). Figure 4(b) is the time dependences of total energy  $E$  and  $Q$  to show the steady states.  $Q(t)$  demonstrates clearly the topological feature of the quantity and its resilience to environmental changes.

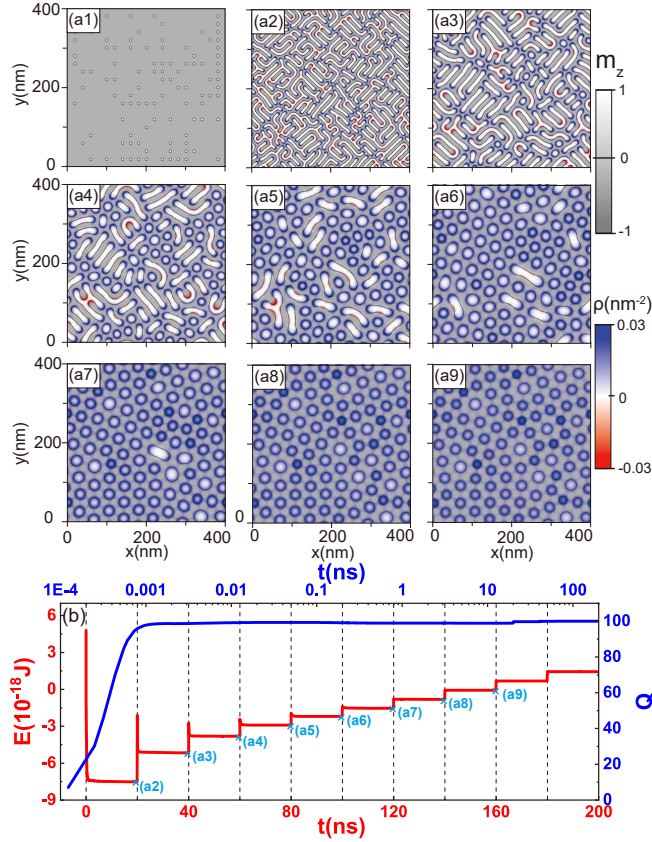


Figure 4: (a1) The initial configuration with 100 randomly distributed nucleation domains of  $m_z = 1$  in the films. The diameter of each domain is 6 nm. (a2)-(a9) The stable structures for  $A/D = 1$  nm at  $t = 20$  ns (a2); 1.5 nm at  $t = 40$  ns (a3); 2 nm at  $t = 60$  ns (a4); 2.5 nm at  $t = 80$  ns (a5); 3 nm at  $t = 100$  ns (a6); 3.5 nm at  $t = 120$  ns (a7); 4 nm at  $t = 140$  ns (a8); 4.5 nm at  $t = 160$  ns (a9).  $\kappa = 2$  is for all films. (b) The time-dependences of skyrmion number  $Q$  (the right y-axis and the blue curve) and the total energy  $E$  (the left y-axis and the red curves). Time  $t$  is in the linear scale for  $E$  (the lower x-axis) and in the logarithmic scale (the top x-axis) for  $Q$ .  $E$  for structures in (a2)-(a9) are marked by cross.  $Q$  reaches 100 within 1 ps and remains this value even when model parameters are tuned.  $E$  approaches its minimal value in nanoseconds after model parameters are tuned.

Our results can either be experimentally tested or be used to explain experiments because magnetic material parameters depend on the temperature. Experiments<sup>58,59</sup> showed that  $A$  and  $D$  de-

depends on  $M$  very differently although mean field theories predict the same dependence of  $A$  and  $D$  on  $M$ . Of course, both  $L$  and  $\kappa$  change with the temperature in realities,<sup>58,59</sup> in contrast to the assumption of constant  $\kappa$  here. Since skyrmion structures are determined by the ratio of  $L$  and skyrmion-skyrmion separation, not on  $\kappa$  as long as it supports condensed skyrmion phase ( $\kappa > 1$ ) such that whether  $\kappa$  is a constant or not is not essential. Beside the temperature, other external knobs such as electrical fields, magnetic fields, as well as strains can also change  $L$ .<sup>60-64</sup>

Physics reported here occurs in the bulk, and should not depend on the boundary conditions. This is also what observed in experiments.<sup>54</sup> However, it is known that helical spin structures ended at a sample edge can be very complicated. Skyrmion numbers of such spin textures are usually not integer. In the Supporting Information, we discuss possible features of textures at sample edges.

Looking forward, our assertion of no first-order phase transition may not be applicable to SkX formation from the closely packed isolated skyrmions. The similarities and differences between the two types of SkXs should be an interesting issue that deserves a careful study. SkXs from a collection of isolated skyrmions due to the skyrmion-skyrmion interaction has many similarities with the formation of atomic crystals through atom-atom interactions. It is well known that the melting or crystallization of an atomic crystal to or from a liquid or an amorphous state is the first-order phase transition involving latent heat. Of course, unlike real crystals in which atoms cannot be destroyed, skyrmion number does not need to be conserved in SkX formation.

In conclusion, a collection of skyrmions transforms into a SkX as the width of stripe skyrmions becomes larger than the skyrmion-skyrmion separation, no matter whether the initial configuration of skyrmions are ordered or randomly distributed in a film and whether the width increases gradually or suddenly. Since the SkX comes from the skyrmion-skyrmion repulsion, it explains why individual skyrmion in a SkX is not a truly circular spin texture. Our finding does not support the notion of the first-order phase transition for SkX formation, but current results cannot rule out the second-order or higher-order phase transitions.

## Methods

Our model is a ferromagnetic film of thickness  $d$  in  $xy$  plane with the total magnetic energy  $E$  consisting of the exchange energy  $E_{\text{ex}}$ , the DMI energy  $E_{\text{DM}}$ , the anisotropy energy  $E_{\text{an}}$ , and the magnetic dipolar energy  $E_{\text{d}}$

$$E = E_{\text{ex}} + E_{\text{DM}} + E_{\text{an}} + E_{\text{d}}, \quad (4)$$

where  $E_{\text{ex}} = Ad \iint |\nabla \mathbf{m}|^2 dS$ ,  $E_{\text{DM}} = Dd \iint [m_z \nabla \cdot \mathbf{m} - (\mathbf{m} \cdot \nabla) m_z] dS$ ,  $E_{\text{an}} = K_u d \iint (1 - m_z^2) dS$ , and  $E_{\text{d}} = \mu_0 M_s d \iint \mathbf{H}_{\text{d}} \cdot \mathbf{m} dS$ .  $M_s$  and  $\mathbf{m}$  are the saturation magnetization and the unit direction of  $\mathbf{M}$ , respectively.  $K_u$  is the perpendicular magneto-crystalline anisotropy and  $\mu_0$  is the vacuum permeability. Magnetization dynamics is governed by the Landau-Lifshitz-Gilbert (LLG) equation,

$$\frac{\partial \mathbf{m}}{\partial t} = -\gamma \mathbf{m} \times \mathbf{H}_{\text{eff}} + \alpha \mathbf{m} \times \frac{\partial \mathbf{m}}{\partial t}, \quad (5)$$

where  $\gamma$  and  $\alpha$  are gyromagnetic ratio and the Gilbert damping constant, respectively.  $\mathbf{H}_{\text{eff}} = \frac{2A}{\mu_0 M_s} \nabla^2 \mathbf{m} + \frac{2K_u}{\mu_0 M_s} m_z \hat{z} + \mathbf{H}_{\text{d}} + \mathbf{H}_{\text{DM}} + \mathbf{h}$  is the effective field including the exchange field, crystalline anisotropy field, demagnetization field, DMI field, and a temperature-induced random magnetic field of magnitude  $h = \sqrt{2\alpha k_B T / (\mu_0 M_s \gamma \Delta V \Delta t)}$  where  $\Delta V$ ,  $\Delta t$ , and  $T$  are the cell volume, time step, and the temperature, respectively. Demagnetization field can be included in the effective anisotropy  $K = K_u - \mu_0 M_s^2 / 2$  when the film thickness  $d$  is much smaller than the exchange length.<sup>13</sup> The thickness of our samples are 0.5 nm which is indeed much smaller than the exchange length of  $\sqrt{2A / (\mu_0 M_s^2)} > 60$  nm, where  $\mu_0 = 4\pi \times 10^{-7}$  N/A<sup>2</sup> is vacuum permeability.

In the absence of energy sources such as an electric current and the heat bath, the LLG equation describes a dissipative system whose energy can only decrease.<sup>65</sup> Thus, the steady state solutions of LLG equation with proper initial magnetization distributions are the stable/metastable spin textures of Eqs. (4). This is an efficient way to find the structure of a skyrmion condensate. Mumax3 package<sup>53</sup> is used to search various metastable spin textures in films of  $400 \text{ nm} \times 400 \text{ nm} \times 0.5 \text{ nm}$  with periodic boundary conditions in both  $x$  and  $y$ -directions. The mesh size is  $1 \text{ nm} \times 1 \text{ nm} \times 0.5 \text{ nm}$

so that no change in simulation results is detected when a smaller mesh size is used. In this study, we consider 10 different films with the same  $M_s = 0.15 \text{ MA/m}$  and  $D = 1 \text{ mJ/m}^2$ .  $A$  and  $K_u$  can vary and are used to tune the stripe width while  $\kappa = 2$  are the same for all 10 films. The values of  $A$  and  $K_u$ , as well as the effective  $K$  are listed in Tab. 1.  $A/D$  of the 10 films varies from 1 nm to 5.5 nm. Also a large  $\alpha = 0.5$  is used to speed up our simulations.

Table 1: The value of material parameters,  $A$ ,  $K_u$ , and  $K$  for 10 different films.

Films	$A(\text{pJ/m})$	$K_u(\text{MJ/m}^3)$	$K(\text{MJ/m}^3)$
1	1.0	0.322	0.308
2	1.5	0.220	0.205
3	2.0	0.168	0.154
4	2.5	0.137	0.122
5	3.0	0.116	0.102
6	3.5	0.102	0.088
7	4.0	0.091	0.077
8	4.5	0.082	0.068
9	5.0	0.075	0.061
10	5.5	0.070	0.056

## ASSOCIATED CONTENTS

### Supporting Information

The Supporting Information is available free of charge on the ACS Publication website at DOI:

- Supporting Information: Discussion of spin structures at sample boundary, damping dependence of metastable state, and determination of the Curie temperatures. (PDF)

## AUTHOR INFORMATION

### Corresponding Author

\*E-mail: phxwan@ust.hk. Phone: +852-23587488. Fax: +852-23581652.

## Notes

The authors declare no competing financial interest.

## ACKNOWLEDGMENTS

This work is supported by the National Key Research and Development Program of China (grant No. 2020YFA0309600), the NSFC (grant No. 11974296), and Hong Kong RGC Grants (No. 16300522, 16301619 and 16302321).

## References

- (1) Bogdanov, A. N.; Röbner, U. K. Chiral Symmetry Breaking in Magnetic Thin Films and Multilayers. *Phys. Rev. Lett.* **2001**, *87* (3), 037203. DOI:10.1103/PhysRevLett.87.037203
- (2) Röbner, U. K.; Bogdanov, A. N.; Pfeiderer, C. Spontaneous skyrmion ground states in magnetic metals. *Nature* **2006**, *442* (7104), 797-801. DOI:10.1038/nature05056
- (3) Mühlbauer, S.; Binz, B.; Jonietz, F.; Pfeiderer, C.; Rosch, A.; Neubauer, A.; Georgii, G.; Böni, P. Skyrmion lattice in a chiral magnet. *Science* **2009**, *323* (5916), 915-919. DOI:10.1126/science.1166767
- (4) Yu, X. Z.; Onose, Y.; Kanazawa, N.; Park, J. H.; Han, J. H.; Matsui, Y.; Nagaosa, N.; Tokura, Y. Real-space observation of a two-dimensional skyrmion crystal. *Nature* **2010**, *465* (7300), 901-904. DOI:10.1038/nature09124
- (5) Yu, X. Z.; Kanazawa, N.; Onose, Y.; Kimoto, K.; Zhang, W. Z.; Ishiwata, S.; Matsui,

- Y.; Tokura, Y. Near room-temperature formation of a skyrmion crystal in thin-films of the helimagnet FeGe. *Nat. Mater.* **2011**, *10* (2), 106-109. DOI:10.1038/nmat2916
- (6) Fert, A.; Cros, V.; Sampaio, J. Skyrmions on the track. *Nat. Nanotech.* **2013**, *8* (3), 152-156. DOI:10.1038/nnano.2013.29
- (7) Sampaio, J.; Cros, V.; Rohart, S.; Thiaville, A.; Fert, A. Nucleation, stability and current-induced motion of isolated magnetic skyrmions in nanostructures. *Nat. Nanotech* **2013**, *8* (11), 839-844. DOI:10.1038/nnano.2013.210
- (8) Nagaosa, N.; Tokura, Y. Topological properties and dynamics of magnetic skyrmions. *Nat. Nanotech.* **2013**, *8* (12), 899-911. DOI:10.1038/nnano.2013.243
- (9) Onose, Y.; Okamura, Y.; Seki, S.; Ishiwata, S.; Tokura, Y. Observation of magnetic excitations of skyrmion crystal in a helimagnetic insulator  $\text{Cu}_2\text{OSeO}_3$ . *Phys. Rev. Lett.* **2012**, *109* (3), 037603. DOI:10.1103/PhysRevLett.109.037603
- (10) Park, H. S.; Yu, X.; Aizawa, S.; Tanigaki, T.; Akashi, T.; Takahashi, Y.; Matsuda, T.; Kanazawa, N.; Onose, Y.; Shindo, D.; Tonomura, A.; Tokura, Y. Observation of the magnetic flux and three-dimensional structure of skyrmion lattices by electron holography. *Nat. Nanotech.* **2014**, *9* (5), 337-342. DOI:10.1038/nnano.2014.52
- (11) Krause, S.; Wiesendanger, R. Spintronics: Skyrmionics gets hot. *Nat. Mater.* **2016**, *15* (5), 493-494. DOI:10.1038/nmat4615
- (12) Rohart, S.; Thiaville, A. Skyrmion confinement in ultrathin film nanostructures in the presence of Dzyaloshinskii-Moriya interaction. *Phys. Rev. B* **2013**, *88* (18), 184422. DOI:10.1103/PhysRevB.88.184422
- (13) Wang, X. S.; Yuan, H. Y.; Wang, X. R. A theory on skyrmion size. *Commun. Phys.* **2018**, *1* (1), 31. DOI:10.1038/s42005-018-0029-0

- (14) Gong, X.; Yuan, H. Y.; Wang, X. R. Current-driven skyrmion motion in granular films. *Phys. Rev. B* **2020**, *101* (6), 064421. DOI:10.1103/PhysRevB.101.064421
- (15) Gong, X.; Jing, K. Y.; Lu, J.; Wang, X. R. Skyrmion pinning by disk-shaped defects. *Phys. Rev. B* **2022**, *105* (9), 094437. DOI:10.1103/PhysRevB.105.094437
- (16) Lenov, A. O.; Monchesky, T. L.; Romming, N.; Kubetzka, A.; Bogdanov, A. N.; Wiesendanger, R. The properties of isolated chiral skyrmions in thin magnetic films. *New J. Phys.* **2016**, *18* (6), 065003. DOI:10.1088/1367-2630/18/6/065003
- (17) Braun, H.-B. Fluctuations and instabilities of ferromagnetic domain-wall pairs in an external magnetic field. *Phys. Rev. B* **1994**, *50* (22), 16485. DOI:10.1103/PhysRevB.50.16485
- (18) Siemens, A.; Zhang, Y.; Hagemester, J.; Vedmedenko, E. Y.; Wiesendanger, R. Minimal radius of magnetic skyrmions: statics and dynamics. *New J. Phys.* **2016**, *18* (4), 045021. DOI:10.1088/1367-2630/18/4/045021
- (19) Simon, E.; Palotás, K.; Rózsa, L.; Udvardi, L.; Szunyogh, L. Formation of magnetic skyrmions with tunable properties in PdFe bilayer deposited on Ir(111). *Phys. Rev. B*, **2014**, *90* (9), 094410. DOI:10.1103/PhysRevB.90.094410
- (20) Karhu, E. A.; Rößler, U. K.; Bogdanov, A. N.; Kahwaji, S.; Kirby, B. J.; Fritzsche, H.; Robertson, M. D.; Majkrzak, C. F.; Monchesky, T. L. Chiral modulations and reorientation effects in MnSi thin films. *Phys. Rev. B* **2012**, *85* (9), 094429. DOI:10.1103/PhysRevB.85.094429
- (21) Iwasaki, J.; Mochizuki, M.; Nagaosa, N. Universal current-velocity relation of skyrmion motion in chiral magnets. *Nat. Commun.* **2013**, *4* (1), 1463. DOI:10.1038/ncomms2442
- (22) Lin, S.-Z.; Reichhardt, C.; Batista, C. D.; Saxena, A. Particle model for skyrmions in metallic chiral magnets: Dynamics, pinning, and creep. *Phys. Rev. B* **2013**, *87* (21), 214419. DOI:10.1103/PhysRevB.87.214419



- (23) Koshibae, W.; Nagaosa, N. Theory of current-driven skyrmions in disordered magnets. *Sci. Rep.* **2018**, *8* (1), 6238. DOI:10.1038/s41598-018-24693-5
- (24) Juge, R.; Je, S.-G.; Chaves, D. de S.; Pizzini, S.; Buda-Prejbeanu, L. D.; Aballe, L.; Forster, M.; Locatelli, A.; Mentès, T. O.; Sala, A.; Maccherozzi, F.; Dhési, S. S.; Auffret, S.; Gautier, E.; Gaudin, G.; Vogel, J.; Boulle, O. Magnetic skyrmions in confined geometries: Effect of the magnetic field and the disorder. *J. Magn. Magn. Mater.* **2018** (1), 455, 3. DOI:10.1038/s41598-018-24693-5
- (25) Kim, J.-V.; Yoo, M.-W. Current-driven skyrmion dynamics in disordered films. *Appl. Phys. Lett.* **2017**, *110* (13), 132404. DOI:10.1063/1.4979316
- (26) Hoshino, S.; Nagaosa, N. Theory of the magnetic skyrmion glass. *Phys. Rev. B* **2018**, *97* (2), 024413. DOI:10.1103/PhysRevB.97.024413
- (27) Woo, S.; Song, K. M.; Zhang, X.; Zhou, Y.; Ezawa, M.; Liu, X.; Finizio, S.; Raabe, J.; Lee, N. J.; Kim, S.-I.; Park, S.-Y.; Kim, Y.; Kim, J.-Y.; Lee, D.; Lee, O.; Choi, J. W.; Min, B.-C.; Koo, H. C.; Chang, J. Current-driven dynamics and inhibition of the skyrmion Hall effect of ferrimagnetic skyrmions in GdFeCo films. *Nat. Commun.* **2018**, *9* (1), 959. DOI:10.1038/s41467-018-03378-7
- (28) Woo, S.; Litzius, K.; Krüger, B.; Im, M.-Y.; Caretta, L.; Richter, K.; Mann, M.; Krone, A.; Reeve, R. M.; Weigand, M.; Agrawal, P.; Lemesh, I.; Mawass, M.-A.; Fischer, P.; Kläui, M.; Beach, G. S. D. Observation of room-temperature magnetic skyrmions and their current-driven dynamics in ultrathin metallic ferromagnets. *Nat. Mater.* **2016**, *15* (5), 501. DOI:10.1038/nmat4593
- (29) Yuan, H. Y.; Wang, X. R. Skyrmion Creation and Manipulation by Nano-Second Current Pulses. *Sci. Rep.* **2016**, *6* (1), 22638. DOI: 10.1038/srep22638
- (30) Zhou, Y.; Ezawa, M. A. Reversible conversion between a skyrmion and a domain-wall pair in a junction geometry. *Nat. Commun.* **2014**, *5* (1), 4652. DOI:10.1038/ncomms5652

- (31) Jiang, W.; Upadhyaya, P.; Zhang, W.; Yu, G.; Jungfleisch, M. B.; Fradin, F. Y.; Pearson, J. E.; Tserkovnyak, Y.; Wang, K. L.; Heinonen, O.; te Velthuis, S. G. E.; Hoffmann, A. Blowing magnetic skyrmion bubbles. *Science* **2015**, *349* (6245), 283-286. DOI:10.1126/science.aaa1442
- (32) Li, J.; Tan, A.; Moon, K. W.; Doran, A.; Marcus, M. A.; Young, A. T.; Arenholz, E.; Ma, S.; Yang, R. F.; Hwang, C.; Qiu, Z. Q. Tailoring the topology of an artificial magnetic skyrmion. *Nat. Commun.* **2014**, *5* (1), 4704. DOI:10.1038/ncomms5704
- (33) Heinze, S.; Bergmann, K. von; Menzel, M.; Brede, J.; Kubetzka, A.; Wiesendanger, R.; Bihlmayer, G.; Blügel, S. Spontaneous atomic-scale Magnetic skyrmion lattice in two dimensions. *Nat. Phys.* **2011**, *7* (9), 713-718. DOI:10.1038/nphys2045
- (34) Dürrenfeld, P.; Xu, Y.; Åkerman, J.; Zhou, Y. Controlled skyrmion nucleation in extended magnetic layers using a nanocontact geometry. *Phys. Rev. B* **2017**, *96* (5), 054430. DOI:10.1103/PhysRevB.96.054430
- (35) Vidal-Silva, N.; Riveros, A.; Escrig, J. Stability of Néel skyrmions in ultra-thin nanodots considering Dzyaloshinskii-Moriya and dipolar interactions. *J. Magn. Magn. Mater.* **2017**, *443*, 116-123. DOI:10.1016/j.jmmm.2017.07.049
- (36) Wilson, M. N.; Butenko, A. B.; Bogdanov, A. N.; Monchesky, T. L. Chiral skyrmions in cubic helimagnet films: The role of uniaxial anisotropy. *Phys. Rev. B* **2014**, *89* (9), 094411. DOI:10.1103/PhysRevB.89.094411
- (37) Romming, N.; Kubetzka, A.; Hanneken, C.; von Bergmann, K.; Wiesendanger, R. Field-Dependent Size and Shape of Single Magnetic Skyrmions. *Phys. Rev. Lett.* **2015**, *114* (17), 177203. DOI:10.1103/PhysRevLett.114.177203
- (38) Du, H.; Che, R.; Kong, L.; Zhao, X.; Jin, C.; Wang, C.; Yang, J.; Ning, W.; Li, R.; Jin, C.; Chen, X.; Zang, J.; Zhang, Y.; Tian, M. Edge-mediated skyrmion chain

- and its collective dynamics in a confined geometry. *Nat. Commun.* **2015**, *6* (1), 8504. DOI:10.1038/ncomms9504
- (39) Romming, N.; Hanneken, C.; Menzel, M.; Bickel, J. E.; Wolter, B.; von Bergmann, K.; Kubetzka, A.; Wiesendanger, R. Writing and deleting single magnetic skyrmions. *Science* **2013**, *341* (6146), 636-639. DOI:10.1126/science.1240573
- (40) Reichhardt, C.; Ray, D.; Olson Reichhardt, C. J. Collective Transport Properties of Driven Skyrmions with Random Disorder. *Phys. Rev. Lett.* **2015**, *114* (21), 217202. DOI:10.1103/PhysRevLett.114.217202
- (41) Yuan, H. Y.; Wang, X. S.; Yung, Man-Hong; Wang, X. R. Wiggling skyrmion propagation under parametric pumping. *Phys. Rev. B* **2019**, *99* (1), 014428. DOI:10.1103/PhysRevB.99.014428
- (42) W. Jiang,; Zhang, X.; Yu, G.; Zhang, W.; Wang, X.; Jungfleisch, M. B.; Pearson, J. E.; Cheng, X.; Heinonen, O.; Wang, K. L.; Zhou, Y.; Hoffmann, A.; te Velthuis, S. G. E. Direct observation of the skyrmion Hall effect. *Nat. Phys.* **2017**, *13* (2), 162–169. DOI:10.1038/nphys3883
- (43) Jaiswal, S.; Litzius, K.; Lemesh, I.; Büttner, F.; Finizio, S.; Raabe, J.; Weigand, M.; Lee, K.; Langer, J.; Ocker, B.; Jakob, G.; Beach, G. S. D.; Kläui, M. Investigation of the Dzyaloshinskii-Moriya interaction and room temperature skyrmions in W/CoFeB/MgO thin films and microwires. *Appl. Phys. Lett.* **2017**, *111* (2), 022409. DOI:10.1063/1.4991360
- (44) Litzius, K.; Lemesh, I.; Krüger, B.; Bassirian, P.; Caretta, L.; Richter, K.; Büttner, F.; Sato, K.; Tretiakov, O. A.; Förster, J.; Reeve, R. M.; Weigand, M.; Bykova, I.; Stoll, H.; Schtz, G.; Beach, G. S. D.; Kläui, M. Skyrmion Hall effect revealed by direct time-resolved X-ray microscopy. *Nat. Phys.* **2017**, *13* (2), 170-175. DOI:10.1038/nphys4000
- (45) Reichhardt, C.; Olson Reichhardt, C. J. Noise fluctuations and drive dependence of

- the skyrmion Hall effect in disordered systems. *New J. Phys.* **2016**, *18* (9), 095005. DOI:10.1088/1367-2630/18/9/095005
- (46) Sampaio, J.; Cros, V.; Rohart, S.; Thiaville A.; Fert, A. Nucleation, stability and current-induced motion of isolated magnetic skyrmions in nanostructures. *Nat. Nanotech.* **2013**, *8* (11), 839-844. DOI:10.1038/nnano.2013.210
- (47) Back, C.; Cros, V.; Ebert, H.; Everschor-Sitte, K.; Fert, A.; Garst, M.; Ma, T. P.; Mankovsky, S.; Monchesky, T. L. ; Mostovoy, M.; Nagaos, N.; Parkin, S. S. P.; Pfliederer, C.; Reyren, N.; Rosch, A.; Taguchi, Y.; Tokura, Y.; von Bergmann, K.; Zang, J. D. The 2020 skyrmionics roadmap. *J. Phys. D: Appl. Phys.* **2020**, *53* (36), 363001. DOI:10.1088/1361-6463/ab8418
- (48) Karube, K.; White, J. S.; Reynolds, N.; Gavilano, J. L.; Oike, H.; Kikkawa, A.; Kagawa, F.; Tokunaga, Y.; Rønnow, H. M.; Tokura, Y.; Taguchi, Y. Robust metastable skyrmions and their triangular–square lattice structural transition in a high-temperature chiral magnet. *Nat. Mat.* **2016** (12), *15*, 1237–1242. DOI:10.1038/nmat4752
- (49) Wang, X. R.; Hu, X. C.; Wu, H. T. Stripe skyrmions and skyrmion crystals. *Commun. Phys.* **2021**, *4* (1), 142. DOI:10.1038/s42005-021-00646-9
- (50) Wu, H. T.; Hu, X. C.; Jing, K. Y.; Wang, X. R. Size and profile of skyrmions in skyrmion crystals. *Commun. Phys.* **2021**, *4* (1), 210. DOI:10.1038/s42005-021-00716-y
- (51) Wu, H. T.; Hu, X. C.; Wang, X. R. Nematic and smectic stripe phases and stripe-SkX transformations. *Science China* **2022**, *65* (4), 247512. DOI:10.1007/s11433-021-1852-8
- (52) Hu, X. C.; Wu, H. T.; Wang, X. R. A theory of skyrmion crystal formation. *Nanoscale* **2022**, *14* (20), 7516-7529. DOI:10.1039/D2NR01300B
- (53) Vansteenkiste, A.; Leliaert, J.; Dvornik, M.; Helsen, M.; Garcia- Sanchez F.; Waeyenberge, F. B. V. The design and verification of MuMax3. *AIP Adv.* **2014**, *4* (10), 107133. DOI:10.1063/1.4899186

- (54) Lin, T.; Wang, C.; Qiu, Z.; Chen C.; Xing, T.; Sun, L.; Liang J.; Wu, Y.; Shi, Z.; Lei, N. Magnetic triangular bubble lattices in bismuth-doped yttrium iron garnet. *Chinese Physics B* **2023**, *32*, 027505. doi:10.1088/1674-1056/aca604
- (55) Kosterlitz, J. M.; Thouless, D. J. Ordering, metastability and phase transitions in two-dimensional systems. *J. Phys. C* **1973**, *6*, 1181. DOI:10.1088/0022-3719/6/7/010
- (56) Halperin, B. I.; Nelson, D. R. Theory of two-dimensional melting. *Phys. Rev. Lett.* **1978**, *41*, (2) 121. DOI:10.1103/PhysRevLett.41.121
- (57) Nelson, D. R.; Halperin, B. I. Dislocation-mediated melting in two dimensions. *Phys. Rev. B* **1979**, *19* (5), 2457. DOI:10.1103/PhysRevB.19.2457
- (58) Zhang, Y.; Kong, X.; Xu, G.; Jin, Y.; Jiang, C. J.; Chai, G. Z. Direct observation of the temperature dependence of the Dzyaloshinskii–Moriya interaction. *J. Phys. D: Appl. Phys.* **2022**, *55* (19), 195304. DOI:10.1088/1361-6463/ac50cd
- (59) Ham, W. S.; Ishibashi, M.; Kim, K.; Kim, S. ; Ono, T. Observation of temperature-dependent Dzyaloshinskii–Moriya interaction within the 50–300 K range. *J. Phys. D: Appl. Phys.* **2022**, *61* (2), 02090. DOI:10.35848/1347-4065/ac46b0
- (60) Schott, M.; Ranno, L.; Béa, H.; Baraduc, C.; Auffret, S.; Bernard-Mantel, A. Electric field control of interfacial Dzyaloshinskii-Moriya interaction in Pt/Co/AlO<sub>x</sub> thin films. *J. Magn. Mater.* **2021**, *520*, 167122. DOI:10.1016/j.jmmm.2020.167122
- (61) Srivastava, T.; Schott, M.; Juge, R.; Křížáková, V.; Belmeguenai, M.; Roussigné, Y.; Bernard-Mantel, A.; Ranno, L.; Pizzini, S. ; Chérif, S.; Stashkevich, A.; Auffret, S.; Boule, O.; Gaudin, G.; Chshiev, M.; Baraduc, C.; Béa, H. Large-voltage tuning of Dzyaloshinskii–Moriya interactions: A route toward dynamic control of skyrmion chirality. *Nano Lett.* **2018**, *18* (8), 4871-4877. DOI:10.1021/acs.nanolett.8b01502

- (62) Deger, C. Strain-enhanced dzyaloshinskii–moriya interaction at Co/Pt interfaces. *Sci. Rep.* **2020**, *10* (1), 12314. DOI:10.1038/s41598-020-69360-w
- (63) Gareeva, Z. V.; Zvezdin, A. K.; Kalyakin, L. A.; Gareev, T. T. Dzyaloshinskii–Moriya interaction, epitaxial strains, phase transitions in multiferroics with cycloidal structure. *J. Magn. Magn. Mater.* **2020**, *515*, 167255. DOI:10.1016/j.jmmm.2020.167255
- (64) Udalov, O. G.; Beloborodov, I. S. Strain-dependent Dzyaloshinskii-Moriya interaction in a ferromagnet/heavy-metal bilayer. *Phys. Rev. B* **2020**, *102* (13), 134422. DOI:10.1103/PhysRevB.102.134422
- (65) Wang, X. R.; Yan, P.; Lu, J.; He, C. Magnetic field driven domain-wall propagation in magnetic nanowires. *Ann. Phys. (NY)* **2009**, *324* (8), 1815-1820. DOI:10.1016/j.aop.2009.05.004

# Graphical TOC Entry

